Pattern dynamics near inverse homoclinic bifurcation in fluids

Pinaki Pal,[1] Krishna Kumar,[2,*] Priyanka Maity,[2] and Syamal Kumar Dana[3]
[1]*Department of Mathematics, National Institute of Technology, Durgapur-713 209, India*
[2]*Department of Physics and Meteorology, Indian Institute of Technology, Kharagpur-721 302, India*
[3]*CSIR-Indian Institute of Chemical Biology, Jadavpur, Kolkata-700 032, India*
(Received 25 August 2012; published 4 February 2013)

We report the pattern dynamics in the vicinity of an inverse homoclinic bifurcation in an extended dissipative system. We observe, in direct numerical simulations of three dimensional Rayleigh-Bénard convection with *stress-free* top and bottom plates, a spontaneous breaking of a competition of two mutually perpendicular sets of oscillating cross rolls to one of two possible sets of oscillating cross rolls as the Rayleigh number is raised above a critical value. The time period of the oscillating cross-roll patterns diverges and shows scaling behavior near the bifurcation point. This is an example of a transition from nonlocal to local pattern dynamics near an inverse homoclinic bifurcation. We also present a simple four-mode model that captures the pattern dynamics quite well.

DOI: 10.1103/PhysRevE.87.023001 PACS number(s): 47.20.Ky, 47.55.pb, 47.20.Bp

I. INTRODUCTION

Extended dissipative systems driven away from thermodynamic equilibrium often form patterns, if the driving force exceeds a critical value [1]. Competing instabilities may lead to interesting pattern dynamics, which helps in understanding the underlying instability mechanism. Several patterns are observed in continuum mechanical systems, such as Rayleigh-Bénard systems [2], Bénard-Marangoni systems [3], magnetohydrodynamics [4], ferrofluids [5], binary fluids [6], granular materials [7] under shaking, biological systems [8], etc. Symmetries and dissipation play a very significant role in pattern selection in such systems [9]. The selection of a pattern is a consequence of at least one broken symmetry of the system. Unbroken symmetries often introduce multiple patterns, which may lead to a transition from local to global pattern dynamics. The gluing [10] of two limit cycles on two sides of a saddle point in the phase space of a given system is an example of a local to nonlocal bifurcation. It occurs when two limit cycles simultaneously become homoclinic orbits of the same saddle point. This phenomenon has been recently observed in a variety of systems including liquid crystals [11], fluid dynamical systems [12], biological systems [13], optical systems [14], and electrical circuits [15], and is a topic of current research. The pattern dynamics in the vicinity of a homoclinic bifurcation has, however, not been investigated in a laterally extended simple fluid dynamical system.

A Rayleigh-Bénard system [16,17], where a thin layer of a fluid is heated uniformly from below and cooled uniformly from above, is a classical example of an extended dissipative system which shows a plethora of pattern-forming instabilities [2], chaos [18], and turbulence [19]. Low-Prandtl-number [20] and very-low-Prandtl-number convection [21,22] show three-dimensional oscillatory behavior close to the instability onset. In addition, the Rayleigh-Bénard system possesses symmetries under translation and rotation in the horizontal plane that can introduce multiple sets of patterns. The possibility of a homoclinic bifurcation and pattern dynamics in its vicinity are unexplored in three-dimensional (3D) Rayleigh-Bénard convection (RBC).

We report, in this article, the pattern dynamics near an inverse homoclinic bifurcation in a laterally extended fluid dynamic system. We have chosen a three-dimensional Rayleigh-Bénard system with *stress-free* (*free-slip*) boundary conditions as a model system for the purpose. The selection of stress-free horizontal boundaries allows the construction of simple models to study pattern dynamics near the homoclinic bifurcation. Direct numerical simulations (DNS) of 3D RBC in low-Prandtl-number fluids show spontaneous breaking of a periodic competition of two mutually perpendicular sets of cross rolls to one set of oscillating cross rolls, as the Rayleigh number Ra is raised above a critical value Ra_h. This is an example of a transition from nonlocal to local oscillatory behavior. The time period of the oscillating patterns diverges and displays scaling behavior in the close vicinity of the bifurcation point. The exponents of scaling are asymmetric on the two sides of the transition point. We also present a simple four-mode model, which captures not only the pattern dynamics in the vicinity of the inverse homoclinic bifurcation but also the whole sequence of bifurcations observed in DNS of RBC quite well over a wide range of Rayleigh number in low-Prandtl-number fluids.

II. HYDRODYNAMICAL SYSTEM AND DIRECT NUMERICAL SIMULATIONS

The hydrodynamics of RBC in a thin layer of Boussinesq fluid of thickness d, kinematic viscosity ν, thermal diffusion coefficient κ, and thermal expansion coefficient α, subjected to an adverse temperature gradient β, is governed by the following dimensionless hydrodynamic equations:

$$\partial_t \mathbf{v} + (\mathbf{v}\cdot\nabla)\mathbf{v} = -\nabla p + \nabla^2\mathbf{v} + \mathrm{Ra}\theta\mathbf{e}_3, \tag{1}$$

$$\mathrm{Pr}[\partial_t\theta + (\mathbf{v}\cdot\nabla)\theta] = \nabla^2\theta + v_3, \tag{2}$$

$$\nabla\cdot\mathbf{v} = 0, \tag{3}$$

where $\mathbf{v}(x,y,z,t) \equiv (v_1,v_2,v_3)$ is the velocity field, $\theta(x,y,z,t)$ the convective temperature field, p the pressure due to convection, and $\mathbf{e}_3$ a unit vector directed against the direction

*kumar@phy.iitkgp.ernet.in

of the acceleration due to gravity **g**. Lengths, time, and temperature are measured in units of the fluid thickness d, viscous diffusion time d^2/ν, and $\nu\beta d/\kappa$, respectively. We use thermally conducting and stress-free boundary conditions which imply that $\theta = v_3 = \partial_z v_1 = \partial_z v_2 = 0$ at $z = 0,1$.

All the fields are assumed to be periodic in the horizontal plane. The Rayleigh number $\mathrm{Ra} = \alpha\beta g d^4/\nu\kappa$ and Prandtl number $\mathrm{Pr} = \nu/\kappa$ are two dimensionless numbers that decide the convective flow structures in the fluid. Convection appears when the reduced Rayleigh number $r = \mathrm{Ra}/\mathrm{Ra}_c$ with $\mathrm{Ra}_c = 27\pi^4/4$ is raised above unity. We integrate the full hydrodynamic system [Eqs. (1)–(3)] for low-Prandtl-number ($\mathrm{Pr} \leqslant 0.025$) fluids using an object-oriented code [23] based on the pseudospectral method. The components of the velocity field $\mathbf{v}(x,y,z,t)$ and the convective temperature field $\theta(x,y,z,t)$ are expanded as

$$v_1(x,y,z,t) = \sum_{l,m,n} U_{lmn}(t) e^{i(lkx+mqy)} \cos(n\pi z), \quad (4)$$

$$v_2(x,y,z,t) = \sum_{l,m,n} V_{lmn}(t) e^{i(lkx+mqy)} \cos(n\pi z), \quad (5)$$

$$v_3(x,y,z,t) = \sum_{l,m,n} W_{lmn}(t) e^{i(lkx+mqy)} \sin(n\pi z), \quad (6)$$

$$\theta(x,y,z,t) = \sum_{l,m,n} \Theta_{lmn}(t) e^{i(lkx+mqy)} \sin(n\pi z). \quad (7)$$

The integers l, m, and n can take values consistent with the equation of continuity [Eq. (3)] and $k = q = k_c = \pi/\sqrt{2}$. The size of the periodic cell for DNS is $2\sqrt{2} \times 2\sqrt{2} \times 1$, and its resolution is $64 \times 64 \times 64$. The time integration is carried out using the standard fourth order Runge-Kutta (RK4) method. The time step is taken as 0.0005 for all the simulations presented here. The simulation was started with random initial conditions, and it was continued until a steady state was reached. The steady state values of fields in a simulation were used as the initial conditions for the next simulation. The value of r was increased in small steps of size Δr ($0.0001 \leqslant \Delta r \leqslant 0.01$) and the numerical simulations were done for several values of r. We also repeated several runs starting with random initial conditions for different values of r and found no hysteresis in the parameter range considered here. The convective dynamics is complex at the primary instability in very low-Prandtl-number fluids [22] due to chaotic flows just above the instability onset. We investigate the pattern dynamics as soon as we observe the first oscillatory pattern close to the onset of convection. Various observed convective patterns in the DNS for $\mathrm{Pr} = 0.01$ and $\mathrm{Pr} = 0$ are listed in the first three columns of Table I.

The first ordered state for $\mathrm{Pr} = 0.01$ appears in the form of a competition of two mutually perpendicular sets of oscillatory cross rolls (OCR-I) which continues to exist until $r = 1.0835$. The first row of Fig. 1 displays the pattern dynamics for $r = 1.076$. It shows the contour plots for the temperature field at $z = 1/2$ in a square box of side $2\lambda_c$, where $\lambda_c = 2\pi/k_c = 2\sqrt{2}$. Two sets of cross rolls, one with $|W_{101}| > |W_{011}|$ and another with $|W_{101}| < |W_{011}|$, appear periodically. The patterns appear as squares when the intensities of the two sets of cross rolls become equal. The periodic competition represents a nonlocal pattern dynamics.

TABLE I. Convective patterns showing nonlocal oscillation of cross rolls (OCR-I), local oscillation of cross rolls (OCR-II), stationary cross rolls (CR), and stationary squares (SQ) computed from direct numerical simulations in two columns in the middle and from a simple model (see Sec. III) in the last column.

Convective	DNS		Model
patterns	$r(\mathrm{Pr} = 0.01)$	$r(\mathrm{Pr} = 0)$	$r(\mathrm{Pr} = 0)$
OCR-I	1.010–1.0835	1.0049–1.0708	1.010–1.0953
OCR-II	1.0836–1.1200	1.0709–1.1315	1.0954–1.1584
CR	1.1210–1.1990	1.1316–1.2005	1.1585–1.2519
SQ	1.2000–1.4200	1.2006–1.4297	1.2520–1.5128

As r is raised above a critical $r_h = 1.0835$, the competing cross rolls (OCR-I) spontaneously break into two possible oscillatory cross rolls (OCR-II). The second and third rows of Fig. 1 show two possibilities of OCR-II for $r = 1.088$. We get oscillating cross-roll patterns with either $|W_{101}| < |W_{011}|$ or $|W_{101}| > |W_{011}|$. Two sets of multiple solutions, which are related by the symmetry $x \to y$ and $y \to x$, continue until $r = 1.120$. Further increase in r leads to the appearance of two sets of stationary cross rolls (CR) at $r = 1.121$ (see Table I), which is observed until $r = 1.199$. Raising the value of r even further leads to a transition from stationary cross rolls to stationary square (SQ) patterns. The upper row of Fig. 2 shows two possibilities of stationary cross-roll patterns at $r = 1.15$, while the lower row of Fig. 2 displays stationary square patterns at $r = 1.35$. A similar sequence is observed in the limit of $\mathrm{Pr} \to 0$ (see Table I). The range of competing cross

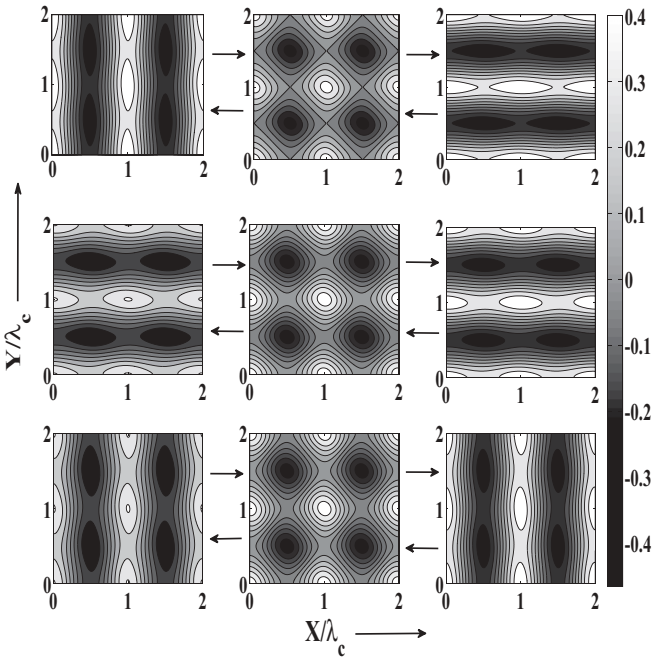

FIG. 1. Contour plots of temperature field at midplane ($z = 0.5$) near an inverse homoclinic bifurcation as observed in DNS ($\mathrm{Pr} = 0.01$). The top row shows competition between two sets of oscillating cross rolls (OCR-I) at $r = 1.076$. The middle and bottom rows show two possibilities of oscillating cross rolls (OCR-II) at $r = 1.088$. The wavelength $\lambda_c = 2\pi/k_c = 2\sqrt{2}$.

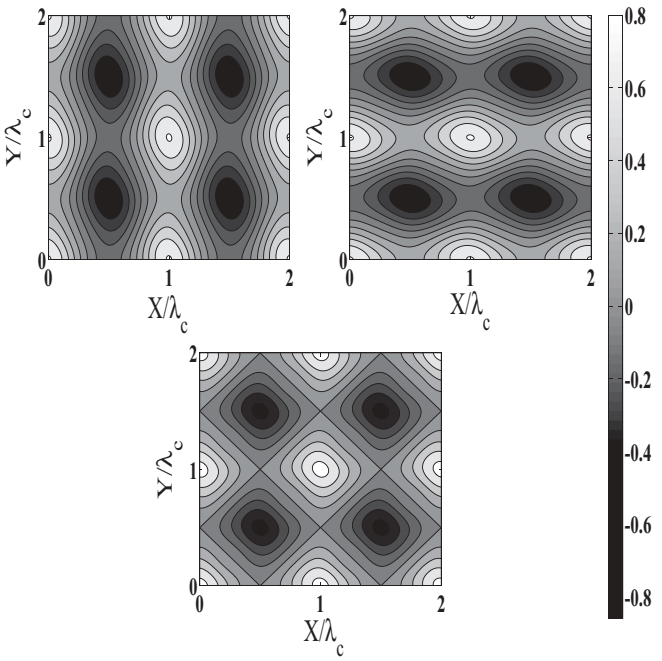

FIG. 2. Contour plots of the temperature field at midplane ($z = 0.5$) displaying two types of stationary cross rolls (CR) at $r = 1.15$ (upper row) and patterns of stationary squares (SQ) at $r = 1.35$ (lower row) as observed in DNS for $\mathrm{Pr} = 0.01$ ($\lambda_c = 2\pi/k_c = 2\sqrt{2}$).

rolls becomes wider as Pr decreases. We have observed the spontaneous breaking of competing cross rolls to two sets of oscillatory cross rolls in fluids with $0 \leqslant \mathrm{Pr} \leqslant 0.025$. Figure 3 shows the details of a transition from global to local pattern dynamics for $\mathrm{Pr} = 0.01$. The divergence of the time period of oscillatory patterns close to the transition point is displayed in Fig. 3(a). The amplitude of the largest Fourier mode of OCR-I patterns decreases linearly with the increase of r and shows two possible values just above the transition ($r = r_h$) point [Fig. 3(b)]. The appearance of two amplitudes signifies a bifurcation from a nonlocal to a local pattern dynamics. The scaling of the time period τ of the oscillating pattern on both sides of the transition point is displayed in Fig. 3(c), showing asymmetry. The time period τ of the competing patterns scales with $\epsilon \equiv |r - r_h|$ as $\epsilon^{-0.115}$ before the transition and as $\epsilon^{-0.0617}$ after the transition. The scaling behavior of the time period of the OCR patterns suggests that the transition is inverse homoclinic. Simulations [21] of low-Pr RBC with no-slip boundaries are known to show relaxation oscillation of patterns.

III. A MODEL

We now construct a simple low-dimensional model to analyze pattern dynamics near the inverse homoclinic bifurcation. For this purpose we take the limit of vanishing Prandtl number ($\mathrm{Pr} \to 0$). As the temperature field is slaved to the vertical velocity, the number of modes representing the effective dynamics is expected to be smaller in this limit. We begin with the standard Galerkin technique to derive a low-dimensional model [22]. We expand the vertical velocity v_3 and the vertical vorticity $\omega_3 \equiv (\nabla \times \mathbf{v})\cdot\mathbf{e}_3$ such that the essential modes to describe two sets of mutually perpendicular rolls, cross rolls, and the nonlinear interaction between them are retained. We keep five velocity modes W_{101}, W_{011}, W_{211}, W_{121}, and W_{112}, and two vorticity modes Z_{110} and Z_{112}. The hydrodynamic equations are projected on these modes. We then adiabatically eliminate modes W_{112}, Z_{110}, and Z_{112}. This leads to a simple four-mode model given by

$$\begin{aligned}\dot{\mathbf{X}} &= \mu_1\mathbf{X} + X_1X_2\mathbb{A}(a_1\mathbf{X} + a_2\mathbf{Y}) + Y_1Y_2\mathbb{A}(a_3\mathbf{X} + a_4\mathbf{Y}) \\ &\quad + a_5\left[X_2^2Y_1, X_1^2Y_2\right]^T + a_6\left[X_1Y_2^2, X_2Y_1^2\right]^T, \\ \dot{\mathbf{Y}} &= \mu_2\mathbf{Y} + X_1X_2\mathbb{A}(b_1\mathbf{X} + b_2\mathbf{Y}) + Y_1Y_2\mathbb{A}(b_3\mathbf{X} + b_4\mathbf{Y}) \\ &\quad + b_5\left[X_2^2Y_1, X_1^2Y_2\right]^T + b_6\left[X_1Y_2^2, X_2Y_1^2\right]^T, \end{aligned} \tag{8}$$

where $\mathbf{X} = [X_1, X_2]^T \equiv [W_{101}, W_{011}]^T$, $\mathbf{Y} = [Y_1, Y_2]^T \equiv [W_{121}, W_{211}]^T$, $\mathbb{A} = [0\ 1; 1\ 0]$, $\mu_1 = 3\pi^2(r-1)/2$, and $\mu_2 = \pi^2(135r - 343)/98$. The coefficients are $a_1 = -3/100$, $a_2 = 31/3000$, $a_3 = -209/30\,000$, $a_4 = 63/60\,000$, $a_5 = -47/1500$, $a_6 = 1/200$, $b_1 = -93/700$, $b_2 = -67/7000$, $b_3 = -7407/70\,000$, $b_4 = -3969/700\,000$, $b_5 = -928/7000$, and $b_6 = 3816/70\,000$. The superscript T denotes the transpose of a matrix. The model is valid for $r < 343/135$ (i.e., $\mu_2 < 0$).

The model is integrated using the standard RK4 method. The time step is taken equal to 0.0005 as is done in the DNS with minimum tolerance 10^{-9}. The third and fourth columns of Table I summarize the results obtained from DNS for $\mathrm{Pr} = 0$ and the model, respectively. The integration is started using

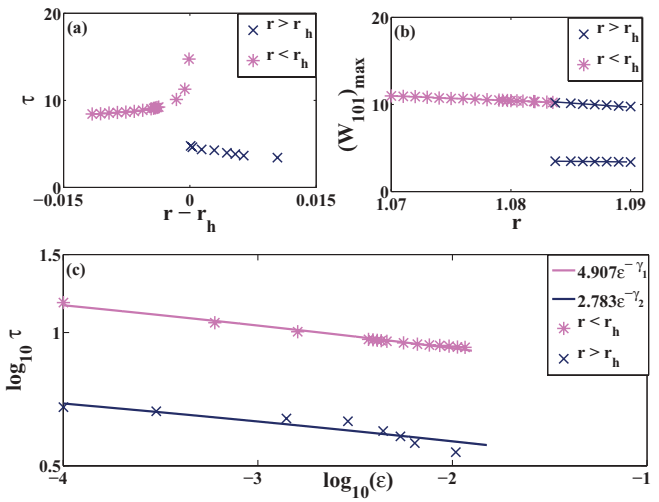

FIG. 3. (Color online) Scaling behavior near an inverse homoclinic bifurcation ($\mathrm{Pr} = 0.01$) as obtained from DNS: (a) The divergence of the dimensionless time period τ of OCR patterns close to the bifurcation point ($r = r_h$) for $r - r_h < 0$ [pink (gray) stars] and for $r - r_h > 0$ [blue (black) crosses]. (b) The variation of maxima of the Fourier mode W_{101} with the reduced Rayleigh number r near the bifurcation, showing the spontaneous transition from a glued oscillation [pink (gray) line] to two possible unglued oscillations [blue (black) line] at the homoclinic point. (c) The scaling of the time period τ of OCR patterns with $\epsilon \equiv |r - r_h|$. The scaling exponents $\gamma_1 = 0.115$ before the transition [pink (gray) line] and $\gamma_2 = 0.0617$ after the transition [blue (black) line] are different. The pink (gray) and the blue (black) lines are the best fits for data points before [pink (gray) stars] and after [blue (black) crosses] the homoclinic bifurcation, respectively.

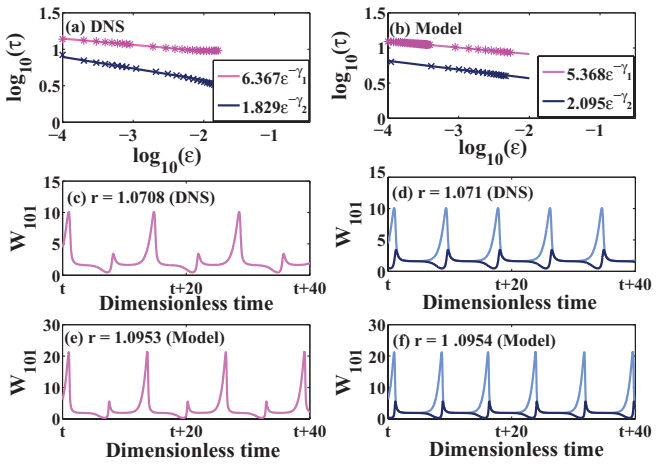

FIG. 4. (Color online) Comparison of results of the model with those from the DNS for Pr = 0: Scaling of dimensionless time period τ of oscillating patterns with $\epsilon \equiv |r - r_h|$ before [pink (gray) line] and after [blue (black) line] the bifurcation, as observed in the DNS (a) and the model (b). The exponents from DNS are $\gamma_1 = 0.086$ and $\gamma_2 = 0.158$, while the exponents from the model are $\gamma_1 = 0.092$ and $\gamma_2 = 0.124$. (c) Temporal variation of the Fourier mode W_{101} [pink (gray) curve] obtained from DNS before the homoclinic bifurcation. (d) Temporal variation of W_{101} showing two possible solutions [light blue (gray) and dark blue (black) curves] just after the bifurcation. (e) Temporal variation of W_{101} [pink (gray) curve] before the bifurcation, and (f) two possible solutions [light blue (gray) and deep blue (black) curves] after the bifurcation, as obtained from the model.

random initial conditions. The reduced Rayleigh number r was increased in small steps as is done in the DNS. Every time r is increased, the steady state field values of the previous run are used as initial conditions for the next value of r. We also checked the results of integration for various values of r starting with random initial conditions. All the results presented here are independent of the choice of the initial conditions. The model captures the sequence of bifurcations quite accurately in a wide range of r as observed in the DNS. The difference in the lower and the upper bounds for the range of r for any solution computed from the model and the DNS is within 6%.

Figure 4 gives the comparison of results obtained from the model and those from DNS for Pr = 0 near a homoclinic bifurcation. The time period τ of competing cross rolls scales with $\epsilon \equiv |r - r_h|$ as $\epsilon^{-\gamma_1}$ before the transition [pink (gray) line] and as $\epsilon^{-\gamma_2}$ after the transition [blue (black) line]. The values of the scaling exponent γ_1 obtained from the DNS [Fig. 4(a)] and the model [Fig. 4(b)] are 0.086 and 0.092, respectively. The DNS and the model yield γ_2 equal to 0.158 and 0.124, respectively. The two exponents are different, showing asymmetry in the scaling behavior on the two sides of the bifurcation point. The values of the two exponents near an inverse homoclinic bifurcation also depend on the value of the Prandtl number Pr. Figure 4(c) displays the temporal variation of the Fourier mode W_{101} [pink (gray) curves] before the homoclinic bifurcation, while Fig. 4(d) shows the temporal variation of the Fourier mode W_{101} [light blue (gray) and dark blue (black) curves] after the bifurcation computed from DNS. Similar behavior is observed in the model [see Figs. 4(e) and 4(f)]. The model reveals that the unstable SQ patterns exist as fixed saddle points for $1 \leqslant r < 1.252$ but become stable at $r = 1.252$. The competing cross rolls (OCR-I) break into two possible sets of OCR-II patterns when the limit cycle describing the OCR-I oscillation touches a saddle square. This confirms the transition from OCR-I to OCR-II as an inverse homoclinic bifurcation. The model includes very few modes, and therefore shows higher values of the Fourier mode W_{101}. The time periods of the oscillating patterns obtained from the model and the DNS are in good agreement both before and after the transition.

IV. CONCLUSIONS

We have investigated the possibility of an inverse homoclinic bifurcation and associated pattern dynamics in RBC with stress-free boundary conditions. The spontaneous breaking of a competition between two mutually perpendicular sets of oscillatory cross rolls into one set of oscillatory cross rolls occurs close to the bifurcation point. The time period of oscillation shows asymmetric scaling on the two sides of the bifurcation point. We have also constructed a simple four-mode model which captures accurately the sequence of bifurcations including the pattern dynamics near the homoclinic bifurcation. The model with different values of the coefficients a_i and b_i may be useful to study pattern dynamics on square lattices in other extended systems with similar symmetries.

ACKNOWLEDGMENTS

We have benefited from fruitful discussions with J. K. Bhattacharjee, H. Pharasi, L.K. Dey, and D. Kumar. S.K.D. is supported by the BRNS/DAE, India (Project No. 2009/34/26/BRNS).

[1] M. C. Cross and P. C. Hohenberg, Rev. Mod. Phys. **65**, 851 (1993).

[2] P. Le Gal, A. Pocheau, and V. Croquette, Phys. Rev. Lett. **54**, 2501 (1985); M. Assenheimer and V. Steinberg, Nature (London) **367**, 345 (1994); H.-W. Xi, X.-J. Li, and J. D. Gunton, Phys. Rev. Lett. **78**, 1046 (1997); K. M. S. Bajaj, J. Liu, B. Naberhuis, and G. Ahlers, *ibid.* **81**, 806 (1998); M. Silber and M. R. E. Proctor, *ibid.* **81**, 2450 (1998); J. Oh and G. Ahlers, *ibid.* **91**, 094501 (2003); F. H. Busse, M. S. Zaks, and O. Brausch, Physica D **184**, 3 (2003).

[3] T. Ondarcuhu, G. B. Mindlin, H. L. Mancini, and C. Perez Garcia, Phys. Rev. Lett. **70**, 3892 (1993).

[4] A. Demircan and N. Seehafer, Geophys. Astrophys. Fluid Dyn. **96**, 461 (2002).

[5] B. Huke and M. Lücke, J. Magn. Magn. Mater. **289**, 264 (2005).

[6] E. Moses and V. Steinberg, Phys. Rev. Lett. **57**, 2018 (1986); S. Weggler, B. Huke, and M. Lücke, Phys. Rev. E **81**, 016309 (2010).

[7] C. Bizon, M. D. Shattuck, J. B. Swift, W. D. McCormick, and H. L. Swinney, Phys. Rev. Lett. **80**, 57 (1998).

[8] L. Yang, A. M. Zhabotinsky, and I. R. Epstein, Phys. Rev. Lett. **92**, 198303 (2004).

[9] J. Guckenheimer and P. Holmes, *Nonlinear Oscillations, Dynamical Systems, and Bifurcations of Vector Fields*, Applied Mathematical Sciences Vol. 42 (Springer-Verlag, New York, 1983); M. Golubitsky and D. G. Schaeffer, *Singularities and Groups in Bifurcation Theories*, Applied Mathematical Sciences Vol. 51 (Springer-Verlag, New York, 1985).

[10] J. Coste and N. Peyraud, Phys. Lett. A **84**, 17 (1981); P. Coullet, J. M. Gambaudo, and C. Tresser, C. R. Acad. Sci. (Paris), Sér. 1: Math. **299**, 253 (1984); J. M. Gambaudo, P. A. Glendinning, and C. Tresser, J. Phys. (France) Lett. **46**, L653 (1985); J. M. Gambaudo, I. Procaccia, S. Thomae, and C. Tresser, Phys. Rev. Lett. **57**, 925 (1986).

[11] G. Demeter and L. Kramer, Phys. Rev. Lett. **83**, 4744 (1999); V. Carbone, G. Cipparrone, and G. Russo, Phys. Rev. E **63**, 051701 (2001); T. Peacock and T. Mullin, J. Fluid Mech. **432**, 369 (2001).

[12] E. Meron and I. Procaccia, Phys. Rev. A **35**, 4008 (1987); J. M. Lopez and F. Marques, Phys. Rev. Lett. **85**, 972 (2000); J. Abshagen, G. Pfister, and T. Mullin, *ibid.* **87**, 224501 (2001).

[13] J. J. Zebrowski and R. Baranowski, Phys. Rev. E **67**, 056216 (2003).

[14] R. Herrero, J. Farjas, R. Pons, F. Pi, and G. Orriols, Phys. Rev. E **57**, 5366 (1998).

[15] P. Glendinning, J. Abshagen, and T. Müllin, Phys. Rev. E **64**, 036208 (2001); P. K. Roy and S. K. Dana, Int. J. Bifurcation Chaos Appl. Sci. Eng. **16**, 3497 (2006).

[16] S. Chandrasekhar, *Hydrodynamic and Hydromagnetic Stability* (Cambridge University Press, Cambridge, 1961); P. Manneville, *Dissipative Structures and Weak Turbulence* (Academic Press, San Diego, 1990).

[17] E. Bodenschatz, W. Pesch, and G. Ahlers, Annu. Rev. Fluid Mech. **32**, 709 (2000), and references therein.

[18] J. P. Gollub and S. V. Benson, J. Fluid Mech. **100**, 449 (1980); A. Libchaber, C. Laroche, and S. Fauve, J. Phys. (France) Lett. **43**, L211 (1982); S. Ciliberto and M. A. Rubio, Phys. Rev. Lett. **58**, 2652 (1987); S. Ciliberto and P. Bigazzi, *ibid.* **60**, 286 (1988); M. C. Cross and Y. Tu, *ibid.* **75**, 834 (1995); J. Liu and G. Ahlers, *ibid.* **77**, 3126 (1996).

[19] L. P. Kadanoff, Phys. Today **54** (8), 34 (2001); M. R. Paul, M. C. Cross, P. F. Fischer, and H. S. Greenside, Phys. Rev. Lett. **87**, 154501 (2001); G. Ahlers, S. Grossmann, and D. Lohse, Rev. Mod. Phys. **81**, 503 (2009); E. M. King, S. Stellmach, J. Noir, U. Hansen, and J. M. Aurnou, Nature (London) **457**, 07647 (2009); H. K. Pharasi, R. Kannan, K. Kumar, and J. K. Bhattacharjee, Phys. Rev. E **84**, 047301 (2011).

[20] G. E. Willis and J. W. Deardorff, J. Fluid Mech. **44**, 661 (1970); F. H. Busse, *ibid.* **52**, 97 (1972); J. Maurer and A. Libchaber, J. Phys. (France) Lett. **41**, 515 (1980); D. R. Jenkins and M. R. E. Proctor, J. Fluid Mech. **139**, 461 (1984); R. E. Ecke, Y. Maeno, H. Haucke, and J. C. Wheatley, Phys. Rev. Lett. **53**, 1567 (1984); Y. Maeno, H. Haucke, and J. C. Wheatley, *ibid.* **54**, 340 (1985); A. Chiffaudel, S. Fauve, and B. Perrin, Europhys. Lett. **4**, 555 (1987); S. Fauve, E. W. Bolton, and M. E. Brachet, Physica D **29**, 202 (1987); Y. Hu, R. E. Ecke, and G. Ahlers, Phys. Rev. Lett. **72**, 2191 (1994); P. K. Mishra, P. Wahi, and M. K. Verma, Europhys. Lett. **89**, 44003 (2010).

[21] O. Thual, J. Fluid Mech. **240**, 229 (1992); E. A. Spiegel, J. Geophys. Res. **67**, 3063 (1962).

[22] K. Kumar, S. Fauve, and O. Thual, J. Phys. II **6**, 945 (1996); P. Pal and K. Kumar, Phys. Rev. E **65**, 047302 (2002); K. Kumar, P. Pal, and S. Fauve, Europhys. Lett. **74**, 1020 (2006); P. Pal, P. Wahi, S. Paul, M. K. Verma, K. Kumar, and P. K. Mishra, *ibid.* **87**, 54003 (2009).

[23] M. K. Verma, arXiv:1103.2517.